
Article:
Palenskis, V, Matukas, J, Pralgauskaite, S et al. (6 more authors) (2013) Low-frequency noise properties of beryllium δ-doped GaAs/AlAs quantum wells near the Mott transition. Journal of Applied Physics, 113 (8). 083707. ISSN 0021-8979

https://doi.org/10.1063/1.4792741

Low-frequency noise properties of beryllium δ-doped GaAs/AlAs quantum wells near the Mott transition

V. Palenskis,[1,a)] J. Matukas,[1] S. Pralgauskaitė,[1] D. Seliuta,[2] I. Kašalynas,[2,3] L. Subačius,[2] G. Valušis,[2,3,b)] S. P. Khanna,[4] and E. H. Linfield[4]
[1]*Radiophysics Department, Vilnius University, Saulėtekio al. 9, LT-10223 Vilnius, Lithuania*
[2]*Optoelectronics Department, Center for Physical Sciences and Technology, A. Goštauto 11, LT-01108 Vilnius, Lithuania*
[3]*Semiconductor Physics Department, Vilnius University, Saulėtekio al. 9, LT-10223 Vilnius, Lithuania*
[4]*Institute of Microwave and Photonics, School of Electronic and Electrical Engineering, University of Leeds, Leeds LS2 9JT, United Kingdom*

(Received 28 January 2013; accepted 5 February 2013; published online 26 February 2013)

Noise properties of beryllium delta-doped GaAs/AlAs multiple quantum wells, doped both above and below the Mott transition, are studied within the frequency range of 10 Hz−20 kHz and at temperature from 77 K to 350 K. It is shown that the generation-recombination noise in structures close to the Mott transition exhibits two peaks—a frequency and temperature-dependent peak between 120 and 180 K and a broadband, frequency- and temperature- nearly independent peak around 270 K. Activation energies are estimated; origin of the broadband maximum is attributed to holes tunnelling into defect trap states located in the AlAs barrier/GaAs quantum well interface.
 [http://dx.doi.org/10.1063/1.4792741]

I. INTRODUCTION

Low-frequency noise spectroscopy is very powerful tool allowing to yield considerable information about nature of physical processes in various materials[1–3] and modern devices.[4–8] Low-frequency noise, such as random telegraph signals (RTS), generation–recombination (GR), and 1/*f*-type noise are related to defects and impurities in materials, in particular to fluctuations of free carriers in the sample owing to their emission and capture by localized states in defects. Superposition of many GR processes with widely distributed characteristic times leads to a 1/*f* noise spectrum, which intensity is proportional to a number of active centers. As a characteristic relaxation time of charge carriers in most cases is thermal activation-related and follows Arrhenius' law, this opens the possibility of making spectroscopic analyses of noise characteristics.[9] For instance, application of low-frequency noise spectroscopy to high-temperature superconducting $YBa_2Cu_3O_7$ films enabled their characterization, determination of fluctuation sources[10] and nonthermal properties;[11] in organic semiconductors low-frequency current fluctuations provide deep insight on trapping-detrapping processes and their characteristic times as well as peculiarities in voltage-driven transition from Ohmic to insulating phase in space-charge-limited conditions.[12] Investigation of noise properties plays a key-role also in development of semiconductor nanostructures-based devices. For example, it is found that photocurrent noise power in photodetectors can be directly related to the carrier density and to photogeneration level, their features can be affected by potential-barrier fluctuations;[13] it is demonstrated that noise gain and photoconductive gain are related in quantum well infrared photodetectors (QWIPs),[14] and inhomogeneous charge distribution in a quantum well (QWs) structure alters intensity and frequency dependence of noise power spectrum.[15]

Doped quantum wells and superlattices are essential components in many photonic devices—both emitters and detectors—designed for very promising in applications terahertz (THz) frequency range.[16] The doping profile and total doping density are key parameters, e.g., in GaAs-based THz quantum cascade lasers, as they strongly influence carrier transport, waveguide losses, and the emission wavelength.[17] Vertical transport in GaAs/AlGaAs doped (QWs) also underpins THz QWIPs, with doping density strongly affecting performance.[18] Doped GaAs/AlAs QWs, both *p*- and *n*-type, can also be used for fast and broadband THz sensing applications through horizontal carrier transport effects.[19,20]

It is well known that impurities in QWs may be distributed smoothly, be tailored to exhibit specific doping profiles, or be concentrated in a sheet, forming so-called δ-doped layer. Nature of the doping in QWs is influenced by the quantum well width, barrier height, impurity position, and concentration. There is a particular interest in highly δ-doped semiconductors or quantum wells—in this case, the nature of the impurity states may change drastically, with strongly interacting impurities forming new states, which can lead to the formation of a two-dimensional carrier gas.[21] The electrical and optical properties of such structures also change, and understanding of these changes is extremely important in the design and development of devices or their components.

In GaAs, beryllium is the acceptor impurity of choice, as it displays relatively low levels of diffusion during growth. From a device standpoint, for instance in *p*-type QWIPs, the strong mixing between the light and heavy holes in the valence band at $k \neq 0$ permits normal incidence absorption, in contrast to *n*-type structures where this is forbidden by

[a)]Electronic mail: vilius.palenskis@ff.vu.lt.
[b)]Electronic addresses: valusis@pfi.lt and gintaras.valusis@ftmc.lt.

quantum-mechanical selection rules.[22] Fabrication of *p*-type QWIPS is therefore more straightforward, however, one needs to understand precisely the effect of the doping level and its profile on the noise (and related) properties of devices, in order to optimize the performance.

Recently, the possible applications of inter-subband transitions in beryllium doped GaAs/AlAs QWs for developing THz sensors and sources has stimulated extensive scientific interest. Acceptor binding energy in δ-doped GaAs/AlAs multiple QWs have been studied,[23] the effect of quantum well confinement on acceptor state lifetime has been investigated,[24] and the dynamics of intra-acceptor level scattering have been examined using far-infrared pump-probe measurements.[25] Application of modulation spectroscopy has allowed estimation of internal built-in electric fields and broadening mechanisms,[26] discrimination between the origin of optical transitions below and close to the Mott transition, and demonstration that with increasing doping level phase space filling effects dominate over the Coulomb screening.[27] Photoluminescence (PL) and time-resolved PL spectra studies have also demonstrated acceptor-impurity induced effects in the (PL) line shapes dependent on the QW widths[28] and allowed one to investigate possible mechanisms for the carrier radiative recombination, both above and below the Mott metal-insulator transition.[29]

In this work, we complement this family of experimental techniques by showing that low-frequency noise measurements are useful method to extract a large variety of information investigating beryllium δ-doped GaAs/AlAs QWs. Through this, it is shown that the generation-recombination noise close to the Mott transition[30] exhibits two peaks—a frequency and temperature-dependent peak between 120 and 180 K, and a broadband, frequency- and temperature- nearly independent peak around 270 K. Activation energies of the former are estimated to range from 0.06–0.27 eV. It is proposed that the origin of the broadband peak is associated with holes tunnelling to trap states located in the AlAs barrier/GaAs quantum well interface.

II. SAMPLES AND EXPERIMENTAL TECHNIQUES

Multiple quantum well (MQW) structures were grown by molecular beam epitaxy on a 1 μm undoped GaAs buffer layer, deposited on a semi-insulating GaAs substrates. The growth temperature for all structures was 650 °C, as measured by an optical pyrometer. Four *p*-type Be-δ-doped structures were studied; all have the same design as in Refs. 29 and 31: the well width is 15 nm, the wells are separated by 5 nm wide AlAs barriers, and each structure consists of 60 periods. The structures differ only in doping concentration at the center of the well: for No. 1, the sheet doping concentration is $n_{Be} = 2.7 \times 10^{11}\,cm^{-2}$, for No. 2—$n_{Be} = 2.7 \times 10^{12}\,cm^{-2}$, for No. 3—$n_{Be} = 2.7 \times 10^{13}\,cm^{-2}$, and for No. 4—$n_{Be} = 5.3 \times 10^{13}\,cm^{-2}$.

Two terminal Ohmic contacts in the samples were fabricated by rapid annealing of Au/Cr alloys.

The spectral density of voltage fluctuations was measured in the frequency range from 10 Hz to 20 kHz at temperature range from 77 K to 350 K. The experimental system contains an extra-low-noise amplifier, filter system and analog-to-digital converter (National Instruments™ PCI 6115 board) (Fig. 1(a)). The noise signal was processed with a computer-based fast Fourier transform signal analyzer, and measurements were performed in a specially shielded room (Faraday cage) in order to avoid interfering effects from electrical network and communication systems.

During the voltage noise measurements, the load resistance was normally selected to be 30-50 times higher than the resistance of the sample in order to operate in a constant current mode. As the resistance of the sample No. 1 is relatively high, for measurements of sample No. 1 below room temperature the noise measurements were performed at constant voltage using a load resistance about 20-40 times smaller than that of the sample. A schematic design indicating the sample configuration and contacts is shown in Fig. 1(b). The voltage fluctuations in the load resistance were then converted into the spectral density of voltage fluctuations of the sample. The spectral density of voltage fluctuations was evaluated by comparison with thermal noise of the reference resistor R_{ref} as follows:

$$S_U = \frac{\overline{V^2} - \overline{V_s^2}}{\overline{V_{ref}^2} - \overline{V_s^2}} 4kT_0R_{ref}, \tag{1}$$

where $\overline{V^2}$, $\overline{V_s^2}$, and $\overline{V_{ref}^2}$ are the sample, measuring system, and reference resistor thermal noise variances, respectively,

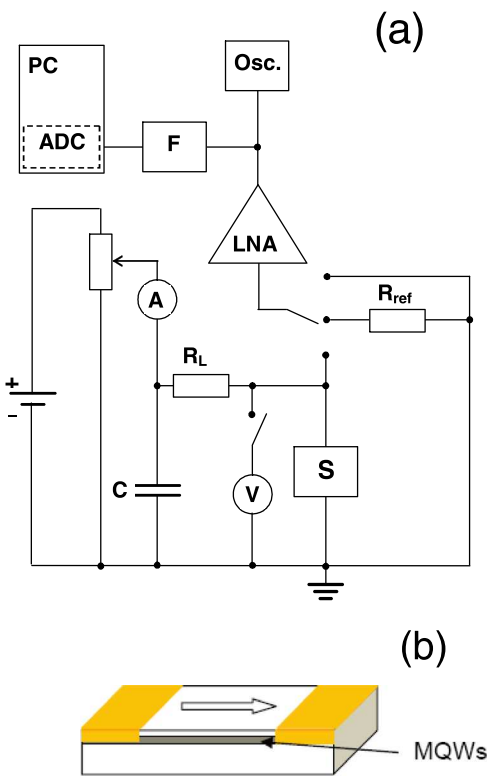

FIG. 1. (a) Experimental apparatus: S—investigated sample, R_L—load resistor, R_{ref}—reference resistor, LNA—low-noise amplifier, F—filter system, ADC—analogue-to-digital converter (National Instrument™ PCI 6115 board), PC—personal computer, Osc.—oscilloscope; (b) schematic design indicating the sample configuration and current flow along the MQWs layers. Yellow areas denote contacts.

in the narrow frequency band Δf; and T_0 is the absolute temperature of the reference resistor.

III. EXPERIMENTAL RESULTS AND DISCUSSIONS

Initially, the structures were characterized electrically. DC current-voltage characteristics (Fig. 2) were measured at room temperature. As expected, different slopes are observed, reflecting the different doping concentrations. Sample No. 1, with the lowest doping level of $2.7 \times 10^{11}\,\mathrm{cm}^{-2}$, displays a shallow slope owing to the relatively high resistance. Sample No. 2, with a doping concentration of $2.7 \times 10^{12}\,\mathrm{cm}^{-2}$, warrants specific attention since its doping concentration is close to the two-dimensional (2D) Mott transition. The experimentally determined value of Be impurities concentration from photoluminescence measurements was found to be $3 \times 10^{12}\,\mathrm{cm}^{-2}$.[31] Theoretically, from the formula[32] $N^{1/2}a_B \approx 0.31$, where N is the critical 2D doping concentration for the Mott transition and a_B is the Bohr radius, the Mott transition for beryllium impurities is at $2.85 \times 10^{12}\,\mathrm{cm}^{-2}$, if one assumes a Be activation energy of 28 meV and the Bohr radius of 2.1 nm.[33] Hence, the doping concentration in sample No. 2 is in the Mott transition region. This can be seen from the dependencies of resistance on temperature (Fig. 3). The variation for sample No. 2 is much weaker than that for sample No. 1, but still noticeable compared with samples No. 3 ($2.7 \times 10^{13}\,\mathrm{cm}^{-2}$), and No. 4 ($5.3 \times 10^{13}\,\mathrm{cm}^{-2}$), where the doping significantly exceeds the Mott transition value.

The dependencies of the measured normalized spectral densities of voltage fluctuations S_U/U^2 (where U is the voltage over the sample terminals) on temperature is presented in Fig. 4 for each sample at different frequencies. For the lightly doped sample (No. 1), the low–frequency noise level in the Mott transition region changes by over four orders of magnitude, but in the temperature range 77 K–210 K, it is almost constant. The low-frequency noise level at low temperatures for sample No. 2, with a doping concentration that is ten times higher, is about two orders of magnitude smaller than that for the sample No. 1. For comparison, the noise levels of two samples with the highest doping concentration (Nos. 3 and 4) are about an order of magnitude smaller below the temperature 200 K. The spectral density dependency on temperature is strongly dependent of the doping level—in particular for sample No. 3: there are peaks in temperature ranges 120 K–180 K and 250 K–300 K. With further

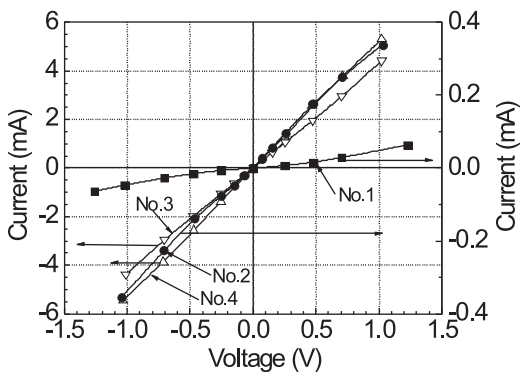

FIG. 2. Current-voltage characteristics of the investigated samples at 290 K.

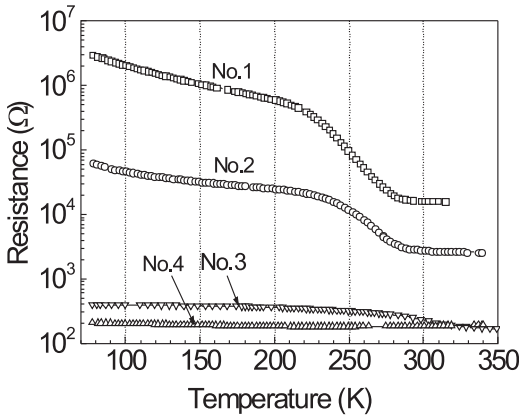

FIG. 3. Resistance of the investigated samples as a function of temperature.

increase in doping (sample No. 4) at lower temperatures the set of peaks moves to the temperature range 100 K–150 K, whilst the higher temperature set of peaks totally disappears. The maxima observed in the temperature ranges 120 K–180 K (for sample No. 3) and 100 K–150 K (for sample No. 4) correspond to GR noise with the spectrum of Lorentzian type[4]

$$\frac{S_U}{U^2} = \frac{a\tau}{1 + (\omega\tau)^2}, \tag{2}$$

where τ is the relaxation time of the GR process; a is the parameter, which defines the GR noise intensity. The maximum of the GR noise level is observed at temperature, when $2\pi f\tau = 1$.

The dashed lines in Fig. 4 show the shift of the maxima of the noise levels for samples Nos. 3 and 4 observed in the temperature range 100 K–180 K to lower temperature with decreasing frequency. The peak observed in temperature range 250 K–320 K is caused by $1/f$-type noise. Similar noise spectra have been observed in MOSFETs at low temperatures and were attributed to real-space transfer effects.[34] One can note that hole tunneling might also be responsible for such noise behavior on temperature, as has already been observed in GaN structures.[35]

In order to obtain a deeper insight into the origin of these noise peaks, we performed additional noise spectra measurements. The low–frequency noise spectra as a function of frequency were measured at fixed temperature points. In this way, characteristic noise spectra at particular temperatures were obtained. Figure 5 shows data for samples Nos. 1 and 2. Figure 6 shows the noise spectra at different temperatures for samples Nos. 3 and 4, where the Lorentzian type spectra are clearly seen. Expanded views to emphasize the details are given in Figs. 6(b) and 6(d).

The noise spectra at low doping (sample No. 1) are of $1/f$–type (flicker noise) nature at all measured temperatures. This type of noise is usually due to superposition of relaxation–like and random pulse processes, and spectral density of such fluctuations can be described in the following way

$$\frac{S_U}{U^2} = \sum_i \frac{a_i\tau_i}{1 + (\omega\tau_i)^2}, \tag{3}$$

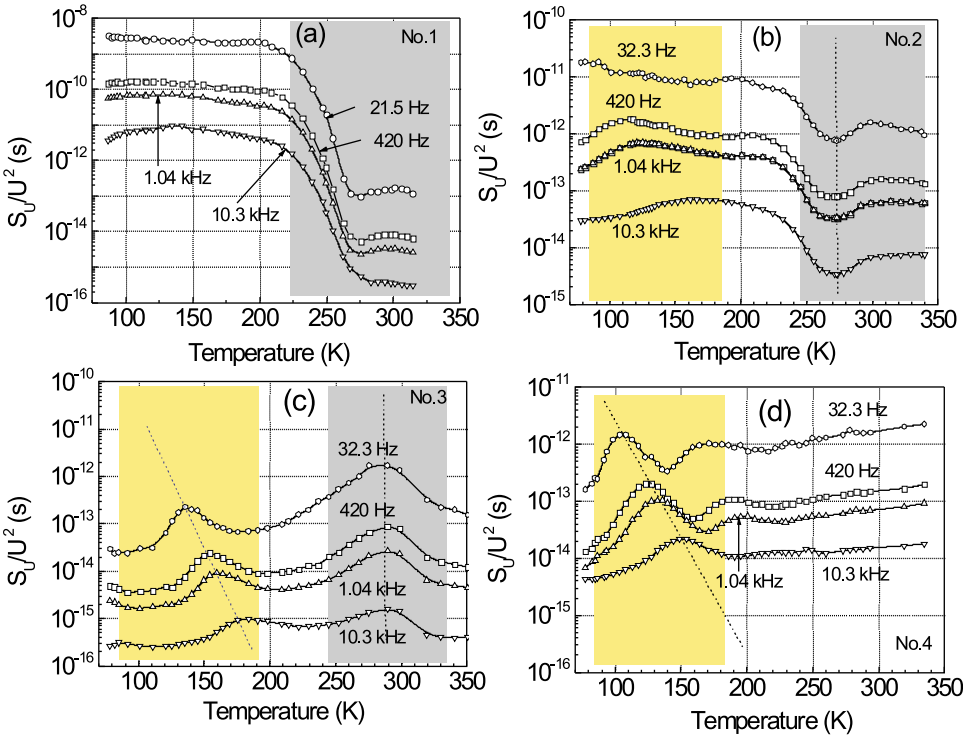

FIG. 4. The dependencies of normalized spectral densities of voltage noise S_U/U^2 on temperature at different frequencies (the sample numbers are given in the diagrams). The dashed lines are a guide to the eye.

where the quantity a_i denotes low-frequency noise intensity and is related to the i-th recombination or capture center density. The distribution of relaxations times, τ_i, explains the low–frequency noise spectrum caused by different charge carrier recombination and/or trapping of energy levels in defects (fluctuators). These defects can be created during growth of the Be-δ-doped GaAs and AlAs layers, and they produce a distortion of the energy of the band gap at interfaces between these layers. Every component of the expression (3), $\omega\tau_i/[1+(\omega\tau_i)^2]$, has a maximum at temperatures when $\omega\tau_i \approx 1$, as it clearly visible from Fig. 7. One can note in addition results of works,[4,36,37] where it was shown that even in high purity silicon single crystal samples there are sufficient number of different recombination and charge carrier capture centers, which cause the 1/*f*–type noise. If the density of the one type of such centers or impurities exceeds the others, the Lorentzian type noise spectra are obtained.

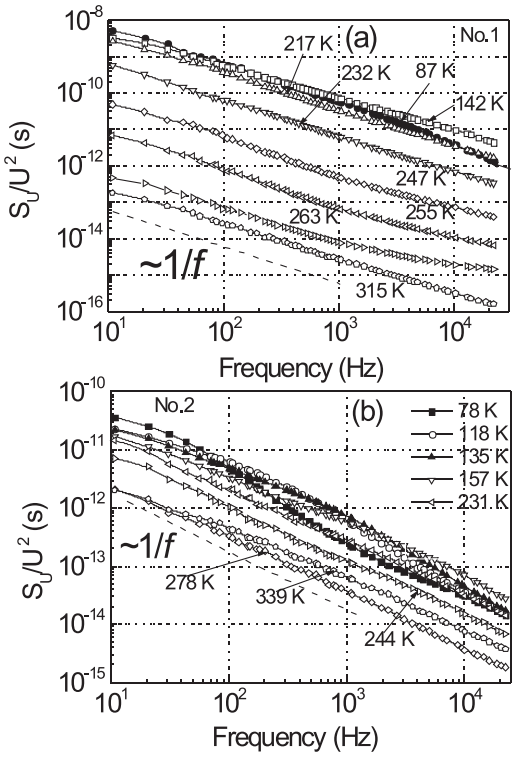

FIG. 5. The low–frequency noise spectra of samples No. 1 and No. 2 at different temperatures.

The maxima obtained allow one to extract characteristic time constants and hence activation energies, assuming that the relaxation times have an activated character

$$\tau_i = \tau_0 \exp(\Delta E^i/kT), \tag{4}$$

where τ_0 is characteristic relaxation time, ΔE^i is the activation energy of the recombination center, and k is the Boltzmann constant.

In order to obtain the recombination (relaxation) time of the charge carriers and their dependence on temperature, it is convenient to multiply the voltage fluctuation spectral density (S_U/U^2) by f. In this case, from the dependence of the peaks of normalized spectral density $(S_U/U^2)f$ on frequency (Fig. 7), one can determine the relaxation time, from $2\pi f_0\tau = 1$ (here f_0 is the frequency of the normalized spectral density peak position on the frequency scale).

The determined relaxation time represents the effective time of charge carrier emission and capture by particular states in the investigated samples, and this dependency on inverse temperature is shown in Fig. 8. The activation energies are also given here. Lorentzian type noise spectra were not found in the sample with the lowest doping concentration (sample No. 1). With the increase of doping density to the range of the Mott transition (sample No. 2), two levels with

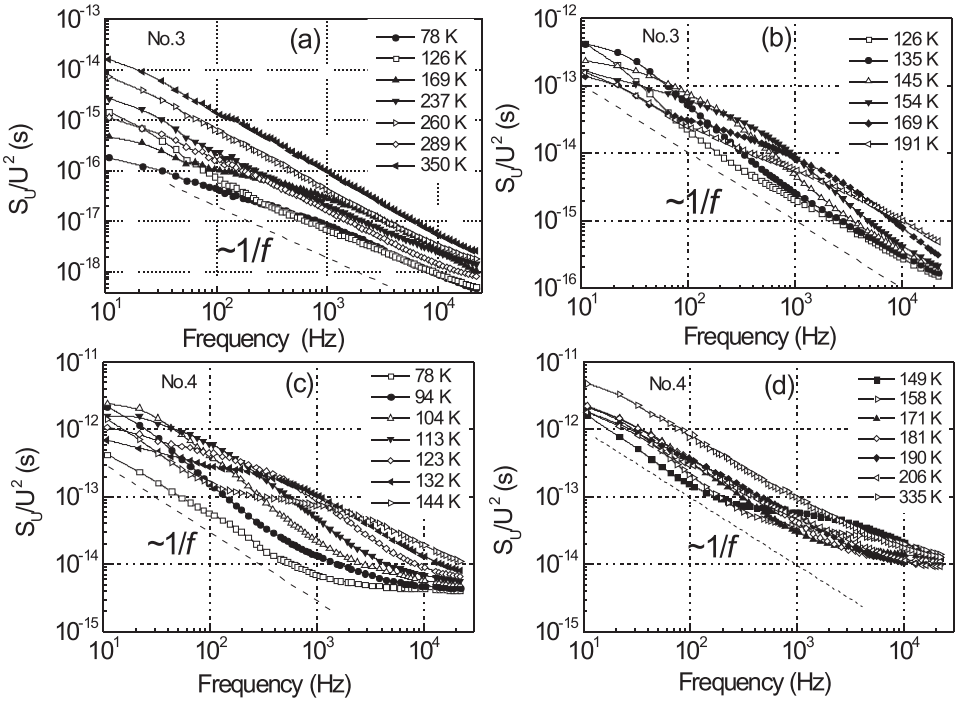

FIG. 6. The low–frequency noise spectra of samples No. 3 and No. 4 at different temperatures with expanded view given in (b) and (d) plots.

activation energies of 0.06 eV and 0.13 eV become pronounced. In sample No. 3 only one level, of 0.27 eV is resolved; in the range of overdoping above the Mott transition (sample No. 4); once again, two levels with energies of 0.11 eV and 0.25 eV can be distinguished.

In order to understand the physics behind these observations and break it down into constituent parts, we quantitatively estimated the energy level structure for high doping levels in the δ-doped layer[38] by numerically calculating the valence band structure using a self-consistent solution of the coupled Poisson and Schrödinger equations.[39,40]

In these calculations, we have used a simple model assuming that the dopant Be acceptors are homogeneously distributed over central part of the 15 nm wide QW. The calculated energy structure of the valence band of the QW for sample No. 3 is shown in Fig. 9. From comparison of the activation energy presented in Fig. 8 with the calculated valence band energy levels, one can conclude that activation energies, obtained from noise spectra measurements are not related to the charge carrier transitions between QW energy levels in the valence band, but have an origin that relates with recombination or trap centers. Analysis of the noise

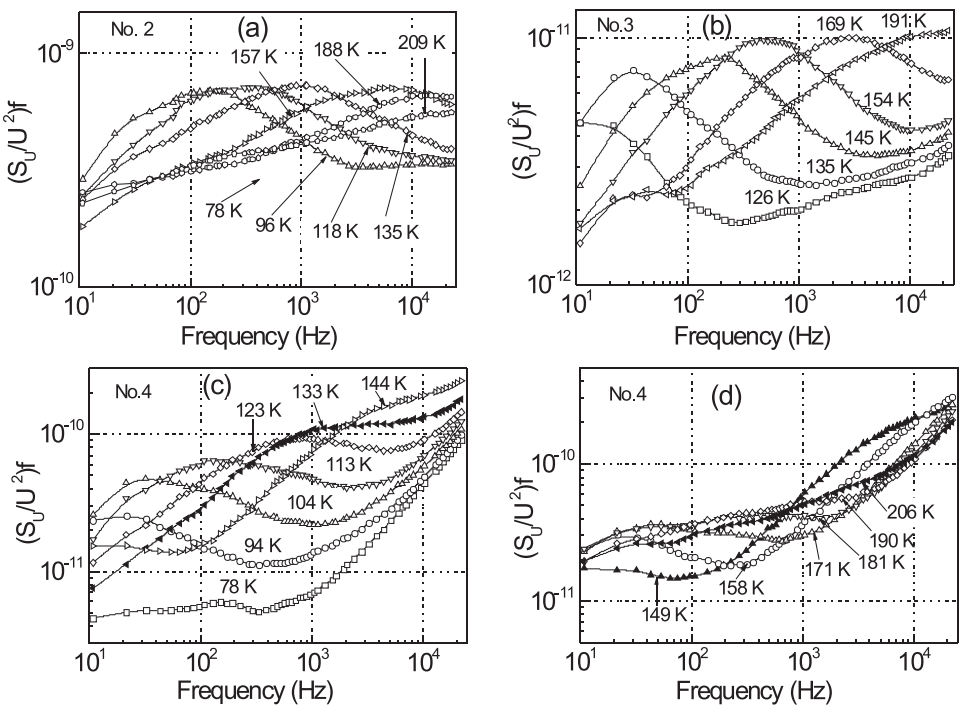

FIG. 7. The normalized noise $(S_U/U^2)f$ spectra of the investigated samples at different temperatures showing Lorentzian type spectra. No activation behavior was found in sample No. 1.

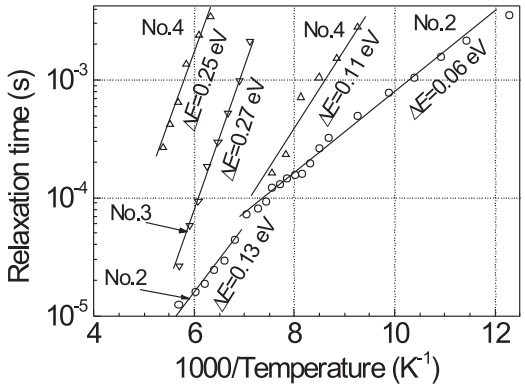

FIG. 8. The charge carrier relaxation time dependencies on temperature and the associated activation energies.

spectra reveals two mechanisms: the first, hole are tunneling[41,42] from Be atoms in a direction that is transverse to the current, i.e. into trap levels located close to the AlAs barrier; the second mechanism, holes are hopping into the other defect level in the GaAs/AlAs barrier interface. One can consider that due to the high doping, the profile of Be-doped δ-layer spreads out[43] from the QW center towards the barriers through the undoped GaAs interface region. When the distance to the interface becomes 4 nm or lower—a distance shorter than the hole tunneling length[44]—light hole tunneling begins to dominate. Hence, holes are extracted from the conductance channel, causing modulation of the resistance of the QW and, as a consequence, producing the low-frequency noise. Note that this process is nearly insensitive of temperature.

The behavior with temperature can also be understood using Fig. 9. At lowest temperature (for instance, at 77 K) the Fermi level is located below all defect levels. Therefore, the occupancy of traps levels is close to zero, and noise is relatively small. With the increase of temperature, the Fermi level moves up, and when it coincides with the relevant

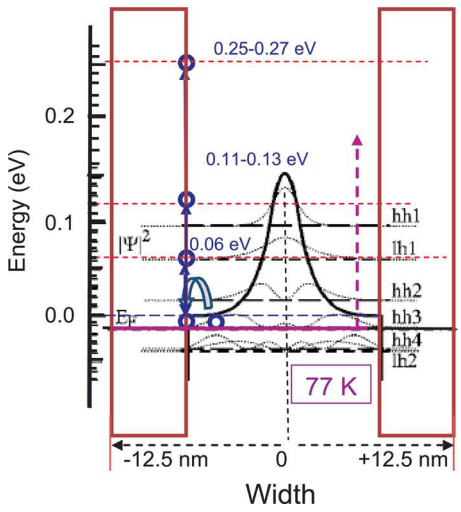

FIG. 9. Simplified schematic diagram of the valence band structure of a highly beryllium doped (sample No. 3, $2.7 \times 10^{13}\,cm^{-2}$) QW at 77 K. The electric blue arrow denotes hole tunneling to the defect state; and the blue arrow shows transitions between the observed defect trap states at the interface labeled by the red dashed lines. The Fermi level is depicted in purple, with the purple dashed arrow showing its shift with temperature.

defect level, occupancy becomes equal to 0.5, and the noise reaches a maximum value (for instance, in Fig. 7, this is $T \approx 190$ K for sample No. 3). With further increase in temperature, increase in the level occupation leads to reduction in the noise.

Since light holes can tunnel to the traps levels in the GaAs/AlAs barrier interface located close to δ-doping layer, the noise spectrum, like in the McWhorter model[45] is of $1/f$ –type (Figs. 5 and 6).

IV. SUMMARY

The noise properties of Be doped GaAs/AlAs QWs, both above and below the Mott transition, have been investigated for temperatures varying from 77 K to 350 K and over the frequency range from 10 Hz to 20 kHz. Frequency- and temperature-dependent contributions to the generation-recombination noise in the structures close to the Mott transition is observed experimentally as a peak in temperature range 120 K-180 K. Estimated activation energies of the trap defect states are in the range from 0.06 eV to 0.27 eV. At temperatures around 270 K a broadband, frequency- and temperature-independent maximum was observed, which is caused by $1/f$ -type noise, and the origin of the broadband peak is attributed to holes tunneling to trap states in AlAs/GaAs interface located close to the beryllium impurity δ-layer, similar to the McWhorter model.

ACKNOWLEDGMENTS

We are very thankful to Alvydas Lisauskas for encouragement of the cooperation; we are grateful to Jurgis Kundrotas, Adolfas Dargys, Julius Kavaliauskas, and Paul Harrison for useful remarks and illuminating discussions.

We acknowledge funding from EPSRC and the European Research Council programme "TOSCA."

[1]R. S. Duran, G. L. Larkins, Jr., C. M. Van Vlieta, and H. Morkoç, J. Appl. Phys. **93**, 5337 (2003).
[2]J. Dobbert, L. Tran, F. Hatami, W. T. Masselink, Vas. P. Kunets, and G. J. Salamo, Appl. Phys. Lett. **97**, 102101 (2010).
[3]G. R. Mutta, J. M. Routoure, B. Guillet, L. Méchin, J. Grandal, S. Martin-Horcajo, T. Brazzini, F. Calle, M. A. Sánchez-García, Ph. Marie, and P. Ruterana, Appl. Phys. Lett. **98**, 252104 (2011).
[4]V. Palenskis, Lith. J. Phys. **20**, 107 (1990).
[5]B. K. Jones, IEEE Trans. Electron Devices **87**, 201 (1994).
[6]V. Palenskis, J. Matukas, K. Maknys, and A. Stadalnikas, in *Proceedings Noise and Reliability of Semiconductor Devices*, edited by J. Sikula and P. Schauer, Brno, (1995), pp. 143–150.
[7]H. Rao and G. Bosman, J. Appl. Phys. **108**, 053707 (2010).
[8]C. Kayis, C. Y. Zhu, M. Wu, X. Li, Ü. Özgür, and H. Morkoç, J. Appl. Phys. **109**, 084522 (2011).
[9]A. Van der Ziel, *Noise in Solid State Devices and Circuits* (Wiley, New York, 1986).
[10]R. P. Black, L. G. Turner, A. Mogro-Campero, T. C. McGee, and A. L. Robinson, Appl. Phys. Lett. **55**, 2233 (1989).
[11]H. S. Kwok, J. P. Zheng, Q. Y. Ying, and R. Rao, Appl. Phys. Lett. **54**, 2473 (1989).
[12]A. Carbone, B. K. Kotowska, and D. Kotowski, Phys. Rev. Lett. **95**, 236601 (2005).
[13]A. Carbone, P. Mazzetti, and F. Rossi, Appl. Phys. Lett. **78**, 2518 (2001).
[14]A. Carbone and P. Mazzetti, Appl. Phys. Lett. **70**, 28 (1997).
[15]A. Carbone, R. Introzzi, and H. C. Liu, Infrared Phys. Technol. **47**, 9 (2005).
[16]M. Tonouchi, Nat. Photonics **1**, 97 (2007).

[17]L. Ajli, G. Scalari, M. Giovannini, N. Hoyler, and J. Faist, J. Appl. Phys. **100**, 043102 (2006).
[18]X. G. Guo, Z. Y. Tan, J. C. Cao, and H. C. Liu, Appl. Phys. Lett. **94**, 201101 (2009).
[19]D. Seliuta, J. Kavaliauskas, B. Čechavičius, S. Balakauskas, G. Valušis, B. Sherliker, M. P. Halsall, P. Harrison, M. Lachab, S. P. Khanna, and E. H. Linfield, Appl. Phys. Lett. **92**, 053503 (2008).
[20]M. Lachab, S. P. Khanna, P. Harrison, E. H. Linfield, A. Čerškus, J. Kundrotas, D. Seliuta, and G. Valušis, J. Cryst. Growth **312**, 1761 (2010).
[21]J. J. Harris, R. Murray, and C. T. Foxon, Semicond. Sci. Technol. **8**, 31 (1993).
[22]B. F. Levine, J. Appl. Phys. **74**, R1 (1993).
[23]W. M. Zheng, M. P. Halsall, P. Harmer, P. Harrison, and M. J. Steer, J. Appl. Phys. **92**, 6039 (2002).
[24]W. M. Zheng, M. P. Halsall, P. Harrison, J.-P. R. Wells, I. V. Bradley, and M. J. Steer, Appl. Phys. Lett. **83**, 3719 (2003).
[25]M. P. Halsall, P. Harrison, J.-P. R. Wells, I. V. Bradley, and H. Pellemans, Phys. Rev. B **63**, 155314 (2001).
[26]B. Čechavičius, J. Kavaliauskas, G. Krivaitė, D. Seliuta, G. Valušis, M. P. Halsall, M. J. Steer, and P. Harrison, J. Appl. Phys. **98**, 023508 (2005).
[27]J. Kavaliauskas, G. Krivaitė, B. Čechavičius, G. Valušis, D. Seliuta, B. Sherliker, M. P. Halsall, P. Harrison, E. H. Linfield, and M. Steer, Phys. Status Solidi B **245**, 82 (2008).
[28]J. Kundrotas, A. Čerškus, S. Ašmontas, G. Valušis, B. Sherliker, M. P. Halsall, M. J. Steer, E. Johannessen, and P. Harrison, Phys. Rev. B **72**, 235322 (2005).
[29]J. Kundrotas, A. Čerškus, G. Valušis, L. H. Li, E. H. Linfield, A. Johannessen, and E. Johannessen, J. Appl. Phys. **112**, 043105 (2012).
[30]N. F. Mott, *Metal-Insulator Transitions* (Taylor & Francis, London, 1974). The Mott transition is defined as the doping limit over which the population of free carriers in the doped material no longer depends on temperature. Above this limit, material is semi-metal: the impurity and conduction bands are degenerate. In δ-doped semiconductors and quantum wells with increasing impurity concentration, the impurity bound states broaden into impurity bands. In p-type doped QWs, in high density limit, the holes are confined to the ionized sheet of the impurities and form a two-dimensional hole gas with a two-dimensional subband structure. More details on features of the Mott transition in QWs can be found in Ref. 33.
[31]J. Kundrotas, A. Čerškus, G. Valušis, M. Lachab, S. P. Khanna, P. Harrison, and E. H. Linfield, J. Appl. Phys. **103**, 123108 (2008).
[32]J. Kortus and J. Monecke, Phys. Rev. B **49**, 17216 (1994).
[33]J. Kundrotas, A. Čerškus, S. Ašmontas, A. Johannessen, G. Valušis, B. Sherliker, M. P. Halsall, P. Harrison, and M. J. Steer, Lith. J. Phys. **45**, 201 (2005).
[34]M. J. Deen, M. E. Levinshtein, S. L. Rumyantsev, and J. Orchard-Webb, Semicond. Sci. Technol. **14**, 298 (1999).
[35]S. L. Rumyantsev, Y. Deng, E. Borovitskaya, A. Dmitriev, W. Knap, M. Pala, M. S. Shur, M. E. Levinshtein, M. A. Khan, G. Simin, J. Yang, and X. Hu, J. Appl. Phys. **92**, 4726 (2002).
[36]Z. Šoblickas and V. Palenskis, Lith. J. Phys. **25**, 88 (1985).
[37]V. Palenskis, J. Matukas, and A. A. Stadalnikas, in *Proceedings of International Workshop*, edited by J. Sikula and P. Shauer, Brno, (1995), pp. 143–150.
[38]P. Harrison, Solid State Commun. **103**, 83 (1997).
[39]I.-H. Tan, G. L. Snider, L. D. Chang, and E. L. Hu, J. Appl. Phys. **68**, 4071 (1990).
[40]P. Harrison, *Quantum Wells, Wires and Dots, Theoretical and Computational Physics* (Wiley, Chichester, 2004).
[41]A. Dargys, J. Phys.: Condens. Matter **9**, L557 (1997).
[42]R. K. Haydeny, T. Takamasuyz, N. Miura, M. Henini, L. L. Eaves, and G. Hill, Semicond. Sci. Technol. **11**, 1424 (1996).
[43]Ph. Ebert, S. Landrock, Y. P. Chiu, U. Breuer, and R. E. Dunin-Borkowski, Appl. Phys. Lett. **101**, 192103 (2012).
[44]V. Palenskis, J. Matukas, and T. Pėstininkas, Lith. J. Phys. **36**, 30 (1996).
[45]A. L. McWhorter, in *Semiconductor Surface Physics*, edited by R. H. Kingston (University of Pennsylvania Press, Philadelphia, PA, 1957), pp. 207–228.